HTC 2012

Capillarity in pressure infiltration: improvements in characterization of high-temperature systems

A. Léger · N. R. Calderon · R. Charvet ·
W. Dufour · C. Bacciarini · L. Weber ·
A. Mortensen

Abstract In the pressure infiltration of metal matrix composites, molten metal is injected under external pressure into a porous preform of the reinforcing material. Equilibrium capillary parameters characterizing wetting for this process are summarized in plots of metal saturation versus applied pressure, also known as drainage curves. Such curves can be measured in our laboratory during a single experiment with an infiltration apparatus designed to track the rate of metal penetration into porous preforms under conditions characteristic of metal matrix composite processing (temperatures in excess of 1000 °C and pressures in the order of 10 MPa). For such measurements to be valid, infiltration of the preform with molten metal must be mechanically quasi-static, i.e., the metal must flow at a rate sufficiently low for the metal pressure to be essentially uniform across the preform at all times. We examine this requirement quantitatively, using a finite-difference model that simulates the unsaturated unidirectional ingress of molten metal into a ceramic particle preform of finite width. We furthermore present improvements in the experimental apparatus developed in our laboratory to measure the entire drainage curve in a single experiment. We compare numerical results with new experimental data for the copper/alumina system to show (i) that pressurization rates sufficiently low for quasi-static infiltration can be produced with this apparatus, and (ii) that taking the relative permeability equal to the saturation yields better agreement with experiment than does the expression originally proposed by Brooks and Corey.

Introduction

Capillary forces are of primary importance in materials processing, and this is particularly true in metal matrix composite (MMC) production by liquid metal infiltration. In this process, molten metal fills a porous *preform* of the reinforcement phase, after which it is solidified within the preform pores, resulting in a composite material. In liquid metal infiltration, capillary forces are typically much higher than gravitational forces. Furthermore, most metals wet poorly most practically interesting reinforcements. Therefore, spontaneous infiltration is rarely observed: external force must generally be applied to drive the molten metal into the preform. As a result, most infiltrated MMCs are produced by pressure infiltration [1–10].

The basic capillary parameter governing infiltration is the work of immersion W_i; this represents the work necessary to wet a unit area of initially dry reinforcement:

$$W_i = \sigma_{SL} - \sigma_{SV} \tag{1}$$

where σ_{SV} and σ_{SL} are the solid–vapor and solid–liquid surface energies, respectively. The work of immersion, W_i, is related to the contact angle, θ, of the metal on the ceramic by the Young equation:

$$\cos \theta = \frac{\sigma_{SV} - \sigma_{SL}}{\sigma_{LV}} = -\frac{W_i}{\sigma_{LV}} \tag{2}$$

A. Léger (✉) · R. Charvet · W. Dufour · L. Weber ·
A. Mortensen
Laboratory of Mechanical Metallurgy, Institute of Materials,
École Polytechnique Fédérale de Lausanne (EPFL),
Station 12, 1015 Lausanne, Switzerland
e-mail: alain.leger@epfl.ch

Present Address:
N. R. Calderon
Philip Morris Products S.A., 2000 Neuchâtel, Switzerland

Present Address:
C. Bacciarini
Innovation Cells, Constellium, 1015 Lausanne, Switzerland

expressing capillary equilibrium at a stationary triple line along a non-deforming solid; here σ_{LV} is the liquid metal surface tension and $\theta > 90°$ indicates a non-wetting system.

The study of wetting, also at elevated temperature, is nearly always associated with the sessile drop experiment. This consists of measuring the equilibrium contact angle θ of a liquid droplet resting on a planar substrate, θ being given by the Young equation (Eq. 2) [11–13]. At elevated temperature, the sessile drop experiment is delicate: challenges that come with high temperatures and the need for tight atmospheric control lead to frequent discrepancies in reported θ values for metal/ceramic systems [12, 14]. With infiltration, furthermore, there is a second difficulty with the technique: a single equilibrium contact angle value is insufficient to fully characterize wetting of a preform by flowing metal, for two reasons. The first is that wetting in infiltration is dynamic: local capillary equilibrium is generally not reached at a moving liquid metal front, which furthermore in pressure infiltration corresponds to forced, rather than spontaneous, wetting. The second has to do with geometry: the invasion by liquid of a complex 3-D labyrinth of irregularly shaped open pores differs from wetting by a drop of a flat surface: molten metals, as most other liquids, invade porous preforms over a range of pressures. This range of pressures, in turn, is dictated by the geometry of open pores within the ceramic preform and by the intensity of capillary forces that equilibrate at a triple line, the exact location of which is a priori unknown. Specifically, with non-wetting liquids, larger pores are invaded first, as these present the smallest resistance to flow, as regards both capillary and viscous forces. Finer pores are only infiltrated later, when the pressure in the metal has reached higher values [2, 5, 8, 15–18].

The importance of capillary forces in infiltration processing of composite materials and particularly in the production of MMCs (given the high value of the liquid surface tension of metals [8]) has motivated a sustained research effort aiming to quantify and hence measure their value. In essence, two basic approaches have been used to characterize wetting of porous preforms by molten metals during infiltration; these are compared in more detail in refs [19, 20].

The first approach explores infiltration under strongly driven flow. Here, experiments are designed to address the fact that wetting in infiltration is dynamic; the capillary number Ca (defined as viscosity times velocity over surface tension) is therefore high. The simplest practical method is to infiltrate unidirectionally a series of samples, varying the pressure while keeping the time fixed. Alternatively, some teams have conducted forced unidirectional infiltration experiments using set-ups that can sense, in

time, the progression of metal into the porous solid body; the ratio of infiltration length squared to time is then measured for a series of (constant) applied pressures. Provided infiltration takes place with a sufficiently well-defined planar infiltration front (something that is called "slug flow"), one can back-calculate by plotting the position of the infiltration front, h, squared versus time, the capillary pressure drop ΔP_γ between the atmosphere and the metal across the infiltration front. From this, making the assumption that infiltration takes place with negligible irreversible energy loss and that behind the infiltration front the preform is fully saturated with liquid metal, the work of immersion W_i (and thus the contact angle θ according to Eq. 2) can be deduced as:

$$\Delta P_\gamma = \frac{V_r A_v W_i}{1 - V_r} = -\frac{V_r A_v \sigma_{LV} \cos\theta}{1 - V_r} \tag{3}$$

where V_r is the volume fraction of reinforcement in the preform and A_v is the reinforcement surface area per unit volume of the reinforcement. Such experiments have been conducted by several laboratories, and when properly conducted and interpreted, gave reliable and consistent results; reviews are given in refs [2, 5, 9].

The other approach addresses the geometrical complexity of porous medium infiltration. Here, experiments are designed to produce the opposite extreme, of very slow infiltration (i.e., low Ca); these are conditions of interest in the present work.

Approaches, aimed at tackling the geometrically complex and gradual nature of infiltration under capillary and mechanical equilibration of the fluids in the pores, come mainly from branches of engineering other than materials science: soil science and petroleum engineering notably [15, 16, 21]. Characterization of pore filling by non-wetting fluids in these disciplines is generally conducted by measurement of *drainage curves*; these are plots of the volume fraction of non-wetting fluid in the porous medium versus the pressure difference ΔP between the liquid and the atmosphere in the pores. Each point along a drainage curve is measured after equilibration, meaning after cessation of fluid flow—in fact, this is what is done at room temperature in a mercury porosimeter. This approach has been extended to high temperatures (e.g., 1000 °C) and high applied pressures (e.g., 10 MPa) characteristic of ceramic–metal systems [17, 18, 22–26]. One method is to infiltrate a series of preforms at different pressures for times long enough that the metal is uniformly distributed throughout the sample, followed by measuring metallographically or by densitometry the volume fraction of metal, and then plot this versus pressure to deduce discrete points along the drainage curve [17, 22, 24]. This discontinuous method is time-consuming and labour-intensive. A far more efficient way is to track dynamically the volume of metal that has

entered the preform (as is practiced in a mercury porosimeter).

The two approaches described above are linked if infiltration of the porous solid preform takes place in both cases (meaning both at high and at low Ca) with negligible irreversible energy loss at the triple line. Then, the drainage curve integrated with respect to saturation of the non-wetting liquid (defined below in Eq. 7), W, should equal the work of immersion, W_i, multiplied by the total area of preform/infiltrant interface created per unit volume of reinforcement, namely

$$W = \int_0^1 \Delta P \, dS = W_i A_v V_r = -\sigma_{LV} \cos\theta A_v V_r$$
$$= (1 - V_r)\,\Delta P_\gamma \tag{4}$$

where ΔP is the pressure difference between the liquid and the atmosphere in the pores at saturation S in the preform after equilibration.

Our laboratory has developed a gas-pressure infiltration apparatus with adequate sensing equipment to provide the entire drainage curve in a single experiment with high-melting point metals such as copper. The system, in its first version, comprised a linear variable differential transformer (LVDT) that was connected (via an alumina tube) to a graphite plunger floating atop the liquid metal. When infiltration starts, the plunger moves with the metal, such that by measuring its displacement, the saturation can be directly deduced as a function of time and pressure. Further details on this infiltration apparatus can be found elsewhere [24]. This technique gave reliable results that matched, at room temperature, those of a mercury porosimeter and, at elevated temperature, those of the discontinuous method for copper infiltrating particulate alumina preforms [24].

We have recently improved this technique, with a goal to ensure quantitatively that infiltration is indeed quasi-static, meaning that, within acceptable precision, the metal volume fraction is uniform across the preform at all times (or in other words that viscous pressure gradients within the liquid are negligible). We present here these improvements, together with a quantitative analysis of the process based on a finite-difference simulation of isothermal infiltration of a rigid preform under an arbitrary increasing-pressure function. Our aim is to define requirements for quasi-static infiltration and to show that these can be met experimentally.

Theory

To quantify requirements for quasi-static isothermal infiltration, a link between the pressure–time history of the infiltration process and the resulting gradients in metal saturation of the pore space must be established. To this end, a finite-difference model was developed to simulate the unsaturated ingress of molten metal into a ceramic particle preform. The physics of the process is similar to drainage phenomena encountered in soil mechanics or reservoir engineering; governing laws can be found in refs [2, 5, 15–17, 23, 27, 28].

The model addresses the unidirectional isothermal infiltration of an evacuated non-deformable inert preform by a non-wetting liquid. Flow of the liquid is governed by continuity (Eq. 5) and Darcy's law (Eq. 6).

$$\frac{\partial V_m}{\partial t} = -\text{div}(v_0) \tag{5}$$

$$v_0 = -\frac{k_e}{\mu}\,\text{grad}(P) \tag{6}$$

where V_m is the local volume fraction of metal, v_0 is the vectorial superficial velocity, μ is the viscosity of the liquid metal, k_e is the porous medium permeability at the relevant local metal saturation, and P is the local pressure (the effect of gravity is generally negligible in metal infiltration [5]). It has been shown [17, 18, 23, 26, 29–32] that quasi-static drainage curves measured at high temperature (discontinuously or continuously) with molten metals and ceramic preforms follow a law known as the Brooks–Corey correlation [16, 28, 33, 34]. This links the capillary pressure P and drainage saturation, according to

$$S \equiv \frac{V_m}{1 - V_r} = 1 - \left(\frac{P_b}{P}\right)^\lambda \tag{7}$$

where S is the saturation in non-wetting liquid (here the metal), V_r is the local volume fraction of reinforcement, and P is the pressure difference between the non-wetting liquid (the metal) and the wetting fluid (the latter being nil since the preforms are initially evacuated). Two parameters underlie the correlation, namely P_b, the "bubbling pressure" (related to the size of the largest pore forming a continuous network) and λ, a "pore size distribution index," which measures the distribution of sizes of the flow channels within the porous medium [16, 27, 28, 33].

In unsaturated flow, the local "effective" permeability k_e is a function of V_m. This can be expressed by taking k_e as the product of the permeability of the fully saturated medium k_s reduced by an S-dependent factor less than unity, known as the relative permeability k_r:

$$k_e = k_r k_s \tag{8}$$

The saturated permeability k_s, characteristic of the preform, can be directly measured, for example by flowing water through the preform (e.g., [35]).

Brooks and Corey [33] also proposed expressions for the relative permeability, k_r, the equation being different for a

wetting or a non-wetting liquid. For a non-wetting liquid, the expression proposed by Brooks and Corey reads

$$k_r = \left[1 - \left(\frac{P_b}{P} \right)^{\lambda} \right]^2 \left[1 - \left(\frac{P_b}{P} \right)^{2+\lambda} \right] \tag{9}$$

Dopler et al. [23] found, on comparing predictions from a model of pressure infiltration with data for aluminum infiltrating preforms of chopped short alumina fibers, that k_r was more adequately predicted by the following simple expression:

$$k_r = S \tag{10}$$

The latter expression, which in Mualem's review corresponds to a Kozeny-type expression with an exponent of unity [36], corresponds in fact to a very simple view of the porous medium, namely one in which the medium is separated into parallel regions much larger than the characteristic pore size, that are either fully filled with liquid or empty. These two expressions for k_r are compared in Fig. 1 : the Brooks and Corey expression supposes a much stronger reduction in permeability with decreasing S than does the linear relation in Eq. (10).

Equation 5 can be rewritten using Eq. (7); after insertion into Eqs. (5) and (6) combined and rewritten in terms of the metal saturation S:

$$\frac{\partial V_m}{\partial t} = \frac{\partial (S(1 - V_r))}{\partial t} = (1 - V_r) \frac{\partial S}{\partial t} \tag{11}$$

One then obtains a single differential equation, which can be written for 1-D linear infiltration along the x direction as:
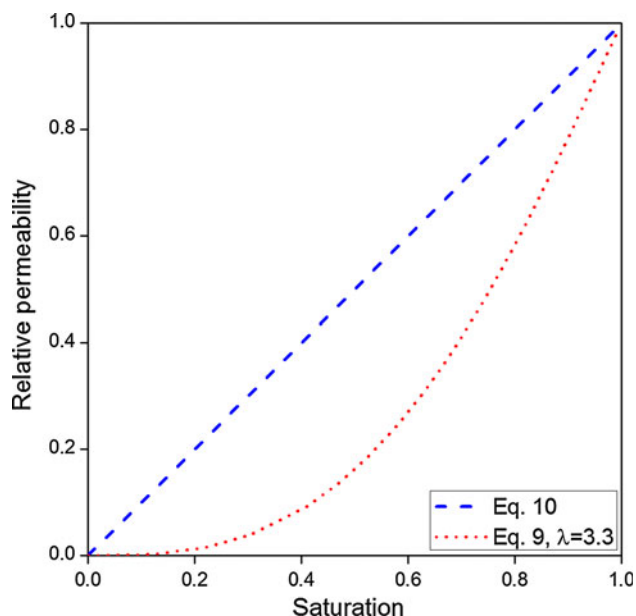

Fig. 1 Relative permeability k_r as a function of saturation S for the expressions given by Eqs. (9) and (10)

$$\frac{\partial S}{\partial t} = \frac{k_s}{\mu (1 - V_r)} \frac{\partial}{\partial x} \left(k_r \frac{\partial P}{\partial S} \frac{\partial S}{\partial x} \right) = \frac{k_s}{\mu (1 - V_r)} \frac{\partial}{\partial x} \left(f(S) \frac{\partial S}{\partial x} \right) \tag{12}$$

and for radial infiltration in cylindrical symmetry as:

$$\frac{\partial S}{\partial t} = \frac{k_s}{\mu (1 - V_r)} \left[\frac{\partial}{\partial r} \left(f(S) \frac{\partial S}{\partial r} \right) + \frac{f(S)}{r} \frac{\partial S}{\partial r} \right] \tag{13}$$

where the term $f(S) = k_r \frac{\partial P}{\partial S}$.

This non-linear equation was solved numerically using the finite-difference method, for an initially dry preform of finite width L, immersed on both sides ($x = 0$ and $x = L$) in liquid metal subjected to a pressure P given as a function of time. The equation was solved using an explicit Euler method for time discretization and a Taylor expansion to first order for the saturation S (in Visual® from Visual C++ Edition Express 2008) by incorporating respectively Eqs. (7), (8) and (9) (or 10) into the code. A slight challenge in designing the code was to devise a suitable method for dealing with the (abrupt) moving infiltration front implied by the Brooks and Corey correlation: precisely at the infiltration front, where P equals P_b, the saturation S and hence $f(S)$ falls to zero. To avoid artificial flow blockage at this point in the calculation, in the explicit finite-difference scheme, $f(S)$ was calculated using the average value of S taken for the two neighbouring nodes. This gives $f(S)$ a finite (albeit at first very small) value at every node situated between the flow entrance point and a distance equal to the distance discretization step Δx times the number of Δt iterations. This did away with a limitation that has often motivated use of the less physically correct but computationally more convenient van Genuchten correlation [37].

Experimental

Materials

Alumina particles were similar to those used in ref [18, 24]. These were of two types, namely (i) angular α-Al_2O_3 F1000 purchased from Treibacher Schleifmittel (Laufenburg, Germany) and (ii) polygonal Sumicorundum AA-5, produced by Sumitomo Chemicals Co., Ltd (Osaka, Japan). Both F1000 and AA-5 alumina powders have an average diameter of around 5 μm. Preforms from the angular F1000 powder were prepared in two different ways: by tapping and vibrating the powder directly into its crucible up to a height of 15 mm, or alternatively by cold isostatic pressing (CIP) at 150 MPa. The obtained CIP preforms were cylindrical, about 14 mm in diameter and 15 mm in height.

The volume fraction of reinforcement ceramic V_r in the preforms (and hence in the composites) was measured by densitometry using a Sartorius MC 210P microbalance of

sensitivity ± 10 μg assuming full infiltration of the composites produced from the preforms. The two packing methods yield volume fractions ceramic $V_r = 0.48$ and 0.53, respectively. The volume fraction ceramic in AA-5 powder preforms pressed by CIP at the same pressure is $V_r = 0.63$.

The saturated permeability k_s of water through tapped F1000 Al_2O_3 preforms was measured experimentally in a polymethyl methacrylate tube equipped with a differential pressure gage and filters retaining the particles at both ends. A series of measurements at pressures in the range of 1–5 bar were conducted by recording the mass of the permeating liquid over 10 min. The permeability was deduced from the measured flow rate using Darcy's law as $k_s = 7 \times 10^{-15}$ m^2 for the tapped F1000 Al_2O_3 preforms, the value varying only little with applied pressure up to 5 bar. Cold isostatically pressed preforms of the same powder have a somewhat higher density; their permeability was estimated by correcting the value measured with tapped preforms for the difference in porosity using the Blake–Kozeny relation [38]. This gave $k_s = 4.2 \times 10^{-15}$ m^2 for the CIPped F1000 Al_2O_3 preforms. Electrolytic tough pitch copper was used as the molten infiltrating matrix. At 1100 °C, its viscosity is 4.3×10^{-3} Pa s, at 1150 °C: 3.9×10^{-3} Pa s, and at 1200 °C: 3.6×10^{-3} Pa s [39].

Gas-pressure infiltration

The gas-pressure infiltration apparatus is a cold-wall device in which heating is provided by an induction coil surrounding a graphite susceptor. A general description of the apparatus is given in [24]. Infiltration is typically conducted in alumina or quartz crucibles; within these a preform is placed below a slug of metal. Once a primary vacuum is established within the apparatus under continued pumping, the metal melts and the preform is sealed from the surrounding atmosphere. After 15 min of thermal equilibration at the infiltration temperature, argon pressure is applied to drive the molten metal into the evacuated preform. Compared to the earlier version of the apparatus described in ref [24], the following modifications were made:

– Use of an automated system for pressure control composed of a set of electrovalves that regulate the gas inlet and outlet up to 20 MPa with 5 kPa precision. This in turn allows for (i) improved precision in control of pressure and (ii) much lower constant pressurization rates.
– A new copper induction coil and graphite susceptor were produced and installed, and the induction heating unit was changed, with the aim to improve heating of the crucible. This was needed to maintain isothermal conditions during prolonged infiltration experiments—

in turn enabling the exploration of much lower pressurization rates. Thermal insulation structures within the apparatus were changed to reduce heat losses and to protect delicate measurement devices from heating, again with a goal to enable experiments of much longer duration.
– An entirely new optical system was built to track motion of the floater, this in turn measuring the metal volume entering into the porous body during infiltration. The main reason for changing the tracking device was that the greater power used in heating for prolonged experiments resulted in a stronger electromagnetic field, the latter in turn perturbing the signal of the LVDT based in the previous system. This was a difficult problem to solve since all commercial measurement devices contain electronic parts, and hence cannot be used in the vicinity of the induction-generated electromagnetic field. A new optical custom-made system was thus conceived and developed, by replacing the adapter formerly containing the LVDT with an adapter featuring two (pressure and vacuum resistant) custom-made windows, one for a light source and the other for capture by a digital camera of a series of white stripes lining the rod that connects the rotative and vibrative systems to the graphite plunger. This in turn allows to track (outside of the magnetic field) the movement of the liquid metal level. The old and the new set-ups are compared in Fig. 2. A dedicated LabView® software was also developed to compute the metal level position by image analysis. The resolution of the system is in the order of several micrometres while the precision (after calibration) is around 40–50 μm for a 6 mm displacement of the graphite plunger.

Infiltration experiments

A first set of drainage experiments were performed to test the precision of the infiltration device. These experiments were conducted with a nominally constant pressurization rate during the entire infiltration run. This was performed for (i) Al_2O_3 (AA-5)/Cu at 0.005 MPa/s and (ii) Al_2O_3 (F1000)/Cu at either 0.04 or 0.005 MPa/s, in both cases at 1200 °C. Experiments with polygonal (AA-5) alumina were done for comparison of the new system with earlier results gathered using the older apparatus.

A second set of drainage experiments were carried out on F1000 alumina preforms only. These were infiltrated with copper under stepwise increasing pressure, holding each pressure level for a time long enough that the displacement of the graphite plunger reached a plateau, or in other words, for the saturation to stabilize. Discrete points in the saturation curve were thus obtained, as in discontinuous experiments—but with the difference that each
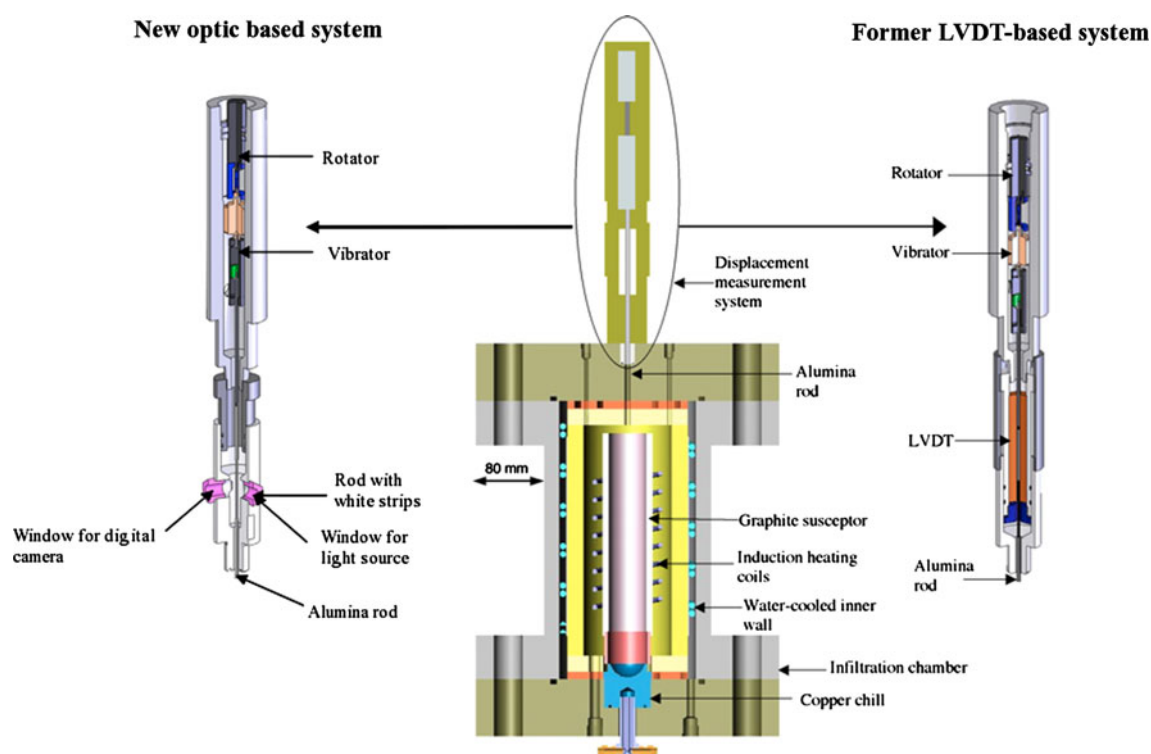
Fig. 2 Schematic of metal level tracking device fixed on top of infiltration apparatus, showing the main differences between the former LVDT-based system (*right*) and the new optic-based system (*left*)

point did not necessitate the preparation and metallographic characterization of a separate sample. Two different types of preforms of F1000 Al_2O_3 were studied in this manner: one preform produced by tapping and vibrating was infiltrated at 1100 °C while the other preform made by CIP was infiltrated at 1150 °C. Note that these two configurations differ in the infiltration path: tapped preforms fill the bottom of the crucible; hence these are mainly infiltrated from the top preform surface downward. CIPped preforms rest on their edges upon the (rounded) bottom of the crucibles; hence these are surrounded by molten metal and infiltrated from all sides simultaneously.

Results

Continuous drainage curves

Figure 3 compares the measured evolution of pressure and temperature versus time during the infiltration of alumina with copper before (a) and after (b) the improvements that were made to the apparatus.

A continuous drainage curve for Al_2O_3 (AA-5)/Cu (0.005 MPa/s) at 1200 °C is displayed in Fig. 4a and compared with results obtained in earlier work [40] for the same system (at 0.04 MPa/s). Figure 4b compares drainage curves for Al_2O_3 (F1000)/Cu, both obtained with the new

apparatus but at two different pressurization rates ($dP_{applied}/dt = 0.04$ and 0.005 MPa/s), also at 1200 °C.

Discontinuous drainage curves

Figure 5 presents discrete points measured after step-wise pressure increases for (i) a preform made of Al_2O_3 (F1000) by tapping and vibrating ($V_r = 0.48$) and (ii) a preform of the same powder made by cold isostatic pressing at 150 MPa ($V_r = 0.53$). Each curve is fitted with the Brooks and Corey (BC) correlation.

Discussion

Improvements to the technique

The difference in precision between the old and the new set-up is clearly illustrated by the data in Fig. 3. With the new apparatus, precise and automatically controlled pressurization rates (here at 10^{-4} and 1.1×10^{-3} MPa/s), as well as temperature (1100 °C $\pm$ 4 °C), remain constant during the whole infiltration process, lasting more than 3 h. These improvements are brought about by the combination of an improved heating system, together with automated and finer pressure and temperature regulation systems. These allow a significantly improved capacity to
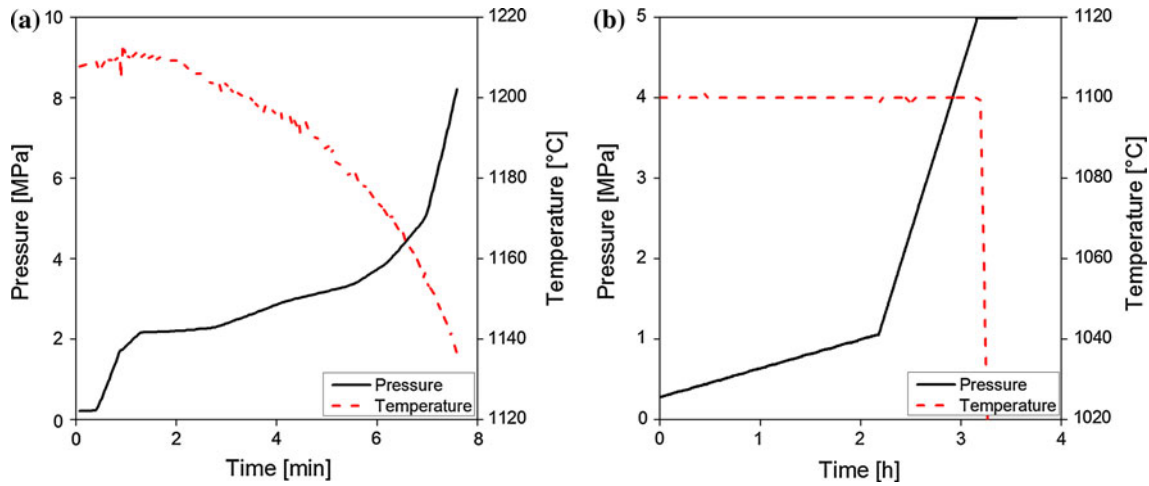
Fig. 3 Typical variation of pressure and temperature as a function of time during two experiments (conducted with the alumina–copper system) using **a** the former [40] and **b** the new set up, in which two different pressurization rates (10^{-4} MPa/s followed by 1.1×10^{-3} MPa/s) were maintained
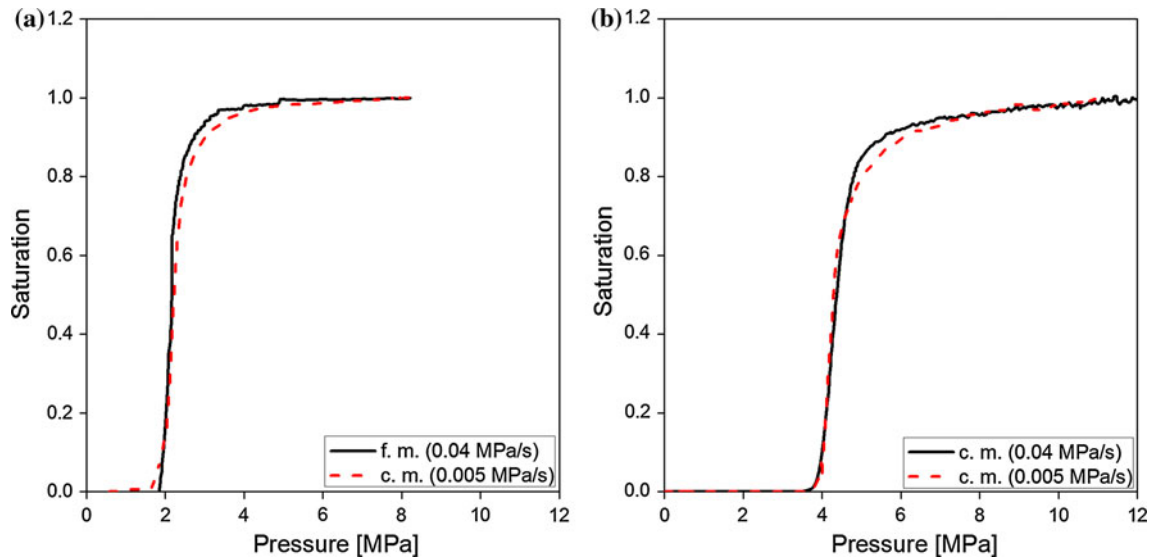

Fig. 4 Drainage curves at 1200 °C for **a** polygonal AA-5 Al$_2$O$_3$/Cu ($V_r = 0.63$) and **b** angular F1000 Al$_2$O$_3$/Cu ($V_r = 0.53$) at 1200 °C, comparing data for two pressurization rate values, d$P_{applied}$/d$t = 0.04$ or 0.005 MPa/s, including data from the present apparatus (c.m.: current method) and former work (f.m.: former method from ref [18]). The preforms were produced by cold isostatic pressing at 150 MPa and $S = 1$ was assumed at 8 MPa for the polygonal AA-5 Al$_2$O$_3$/Cu and at 11 MPa for angular F1000 Al$_2$O$_3$/Cu

compensate for two main factors: (i) ingress of pressurized cold gas into the chamber at high temperature produces a decrease of temperature, (ii) starting around 2–4 MPa gas pressure, heat losses by conduction and convection through the gas to the cooled walls of the pressure infiltration apparatus become important.

Figure 4a compares data collected before (f.m.) and after (c.m.) modifications of the system. Good agreement is obtained, confirming that both methods can generate reliable drainage curves; however, improvements to the apparatus now allow to work in a much broader range of experimental conditions, including pressurization rates

spanning the range from 10^{-1} to 10^{-4} MPa/s while maintaining high temperatures stable within a few degrees (± 5 °C at 1300 °C). Such slow infiltration under stable thermal conditions was not feasible with the older version of the apparatus.

Pressurization rate for quasi-static infiltration under continuous pressurization

Suitable computing parameters (in terms of step size ($\Delta x = 2.5 \times 10^{-3}$ m) and stability ($\Delta t = 10^{-5}$ s) for isothermal unidirectional infiltration under constant pressure
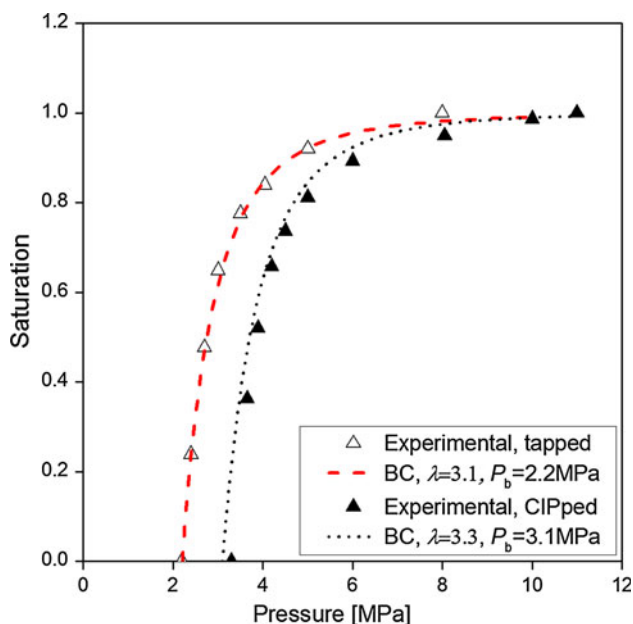
Fig. 5 Drainage curves for angular Al_2O_3 (F1000)/Cu **a** with a preform made by tapping and vibrating ($V_r = 0.48$) at 1100 °C and **b** a preform made by cold isostatic pressing at 150 MPa ($V_r = 0.53$) and infiltrated at 1150 °C. Each curve is fitted with the Brooks and Corey correlation (Eq. 7; see Fig. 7) for appropriate P_b and λ. $S = 1$ was assumed at 8 MPa for the tapped preform and at 11 MPa for the CIPed preform
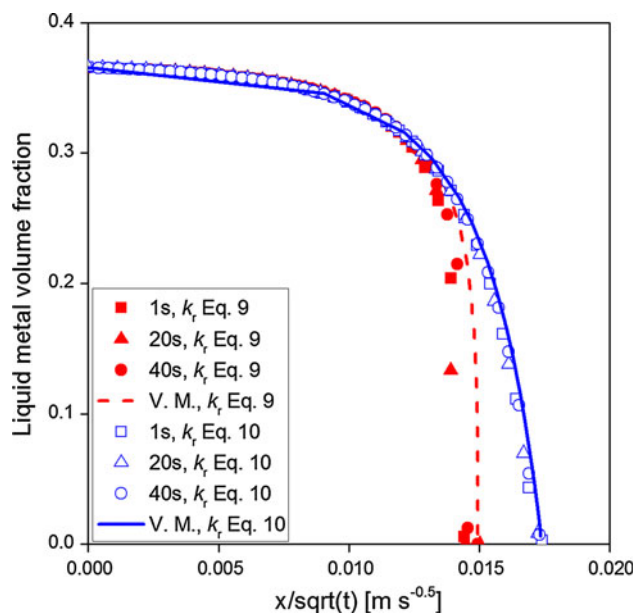

Fig. 6 Comparison of the semi-analytical similarity solution ("V.M.", calculated by Prof. V. Michaud of EPFL) and finite-difference numerical simulation results for unidirectional infiltration according to the Brooks and Corey saturation model (Eq. 7) conducted for k_r from Eq. (9) (*full red symbols, dotted red line*) or Eq. (10) (*hollow black symbols, full black line*), with a constant inlet pressure P_0 after 1, 20, and 40 s ($P_0 = 5$ MPa, $\lambda = 4.9$, $P_b = 2$ MPa, $k_s = 5 \times 10^{-14}$ m^2, $\mu = 3 \times 10^{-3}$ Pa s, $V_r = 0.63$); abscissa is the similarity solution variable, namely distance divided by the square root of time (Color figure online)

P_0 were first identified, by comparison of predictions to those of a semi-analytical solution based on the similarity solution method, which holds for infiltration of semi-infinite media under constant pressure (calculated by Prof. V.J. Michaud, EPFL, as described in refs [17, 20]) with k_r from Eqs. (9) or (10), Fig. 6. The good agreement validates the present finite-difference model, which was then used to simulate infiltration under variable increasing pressure.

The Brooks and Corey parameters inputted in the code are calculated from Fig. 5 for each of the two preform types. Replotting these data in the appropriate coordinates—log $(1 - S)$ versus log (P)—should lead to a straight line if the Brooks and Corey relation for saturation is obeyed. One finds that Eq. (7) is indeed followed by the data, Fig. 7. The two parameters of the correlation (P_b and λ) can then be deduced as $P_b = 2.2$ MPa with $\lambda = 3.1 \pm 0.1$ for F1000 alumina preforms made by tapping and vibrating, and $P_b = 3.1$ MPa with $\lambda = 3.3 \pm 0.1$ for F1000 alumina preforms made by CIP (uncertainties in λ given above were evaluated according to ref. [41]). This fact that λ takes (within error) the same value for both preforms is expected, given that these were made of the same powder. The same was already observed in ref. [18] and confirms that λ reflects mostly the particle shape, as was initially proposed by Brooks and Corey [33] (we note

in passing that a nominally similar F1000 alumina powder used in earlier experiments gave a slightly different λ value in the range 2.6–2.9 [40]).

If one assumes that P_b scales with the work of immersion [18, 24], when V_r is increased from 0.48 to 0.53 the corresponding lines should be shifted horizontally by a factor of

$$\frac{V_r^{CIPped}}{V_r^{tapped}} \times \frac{1 - V_r^{tapped}}{1 - V_r^{CIPped}} = \frac{0.53}{0.48} \times \frac{0.52}{0.47} \approx 1.2 \quad (14)$$

which is near, albeit somewhat lower than, the measured shift, which corresponds to a factor nearer 1.4. Cold-pressing having damaged some particles, the 50 °C difference in infiltration temperature plus uncertainty in the measurements might explain the discrepancy.

Simulations were then performed, using alternatively the relative permeability k_r given in Eq. (9) or that given in Eq. (10). Cold isostatically pressed preforms of Figs. 5 and 7 were considered; we assumed these to be infiltrated radially from the outer preform surface inward with an outer preform diameter of 14 mm, for each of the two pressurization rates of Fig. 4 (0.04 and 0.005 MPa/s). Figure 8 illustrates the effect that the adopted expression
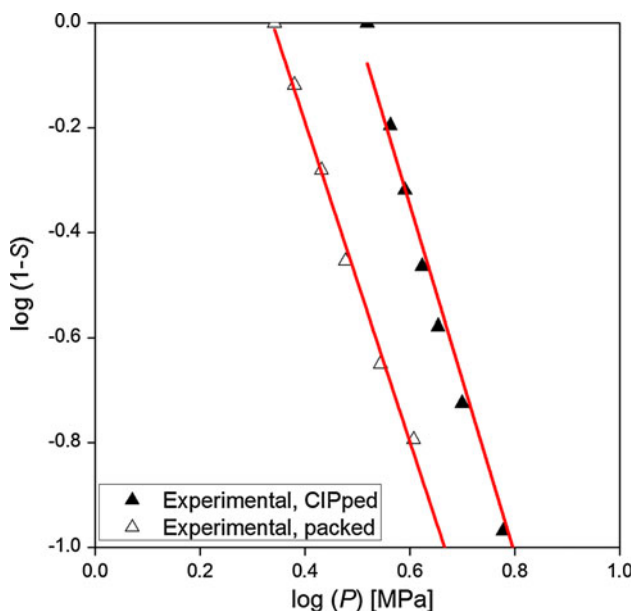
Fig. 7 Same curve as Fig. 5, replotted in terms of the Brooks–Corey correlation. $P_b = 2.2$ MPa and $\lambda = 3.1$ for the preform made by tapping and vibrating and $P_b = 3.1$ MPa and $\lambda = 3.3$ for the preform made by CIP

for k_r has on the numerical predictions. This figure plots, for these two pressurization rates:

(i) the saturation profile at three different instants (Fig. 8a, b), and

(ii) the resulting curves of measured apparent saturation (i.e., the average saturation corresponding to the total volume of metal infiltrated into the preform at time t) versus pressure. These curves are also compared with the Brooks–Corey saturation expression used in the calculation (Eq. 7 with parameters given above from Figs. 5, 7) for quasi-static infiltration (Fig. 8c, d).

As seen, the relative permeability value k_r exerts a strong influence on predicted infiltration kinetics, especially at lower pressure, i.e., near P_b. Each drainage curve presents, indeed, a deviation (more or less accentuated) from the quasi-static Brooks and Corey saturation expression, Fig. 8c and d. Using k_r from Eq. (10) leads to the prediction that the saturation is essentially uniform across the preform at all times with a pressurization rate of 0.005 MPa/s, which hence reproduces faithfully the assumed "real" saturation curve (red "BC" line in Fig. 8c, d). At 0.04 MPa/s the saturation takes longer to become uniform; still, the curve traces, at higher pressures, a significant portion of the "real" (Brooks and Corey) saturation curve.

As the relative permeability k_r defined from the Brooks and Corey correlation (Eq. 9) is lower than k_r from Eq. (10) for the same saturation as well as decreases more rapidly with decreasing S (Fig. 1), using this expression instead of

Eq. (10) will predict much slower and less homogeneous infiltration. This is seen in Fig. 8, where strong gradients are predicted with this expression and where a pressurization rate of 0.04 MPa/s largely underestimates the quasi-static drainage curve up to a saturation of 0.7. Experimental data on the other hand show no significant difference between drainage curves collected at 0.04 or 0.005 MPa/s, Fig. 4. This suggests that Eq. (9) is not suitable in the present copper/alumina system, while Eq. (10) seems to produce adequate predictions. This agrees with the findings of ref [23], who proposed Eq. (10) by comparison of their simulation with data for aluminum infiltrating chopped alumina fibre preforms.

Isobaric infiltration

Calibrating the model with relevant values of P_b and λ for the two preform types (Figs. 5, 7), predictions of the unidirectional infiltration model can also be compared with data from the two infiltration experiments that produced the data in Fig. 5. Note that in the former case infiltration is assumed to take place from the top only; hence unidirectional infiltration of a finite slab was simulated, its thickness L being taken as twice the preform height, namely 30 mm (in Cartesian coordinate system). With CIPped preforms, on the other hand, since the preform is freestanding within the crucible, radial infiltration of the cylindrical preforms was assumed, the preform diameter being 14 mm. Figure 9 compares the numerical (calculated with k_r from Eqs. 9 or 10) and experimental saturation versus time for pressure ramps in these two stepwise infiltration experiments.

As seen in Fig. 9a, best fit for packed preform is again obtained using k_r from Eq. (10) while with Eq. (9) (k_r from the Brooks and Corey correlation), numerical results underpredict significantly the infiltration rate for P values near P_b (lower part of the curves in Fig. 9a). Above $S = 0.5$, the infiltration kinetics for both numerical approaches are the same. Simulation of the CIPped preform, on the other hand, predicts much faster infiltration than is observed at low pressure, also when k_r is calculated according to Eq. (10). We have at present no simple explanation for the discrepancy, which we are currently investigating by conducting more experiments.

More work, both theoretical and experimental, is thus needed; however, it emerges from the present comparison that the Brooks and Corey expression for the relative permeability, Eq. (9), is an underestimate of the permeability of the present ceramic preforms to flowing (strongly nonwetting) metal. Comparatively, a relative permeability equal to saturation (Eq. 10) gives a better approximation. In this connection, it is also worth noting that the Brooks and Corey correlation is likely to be unsuitable at low
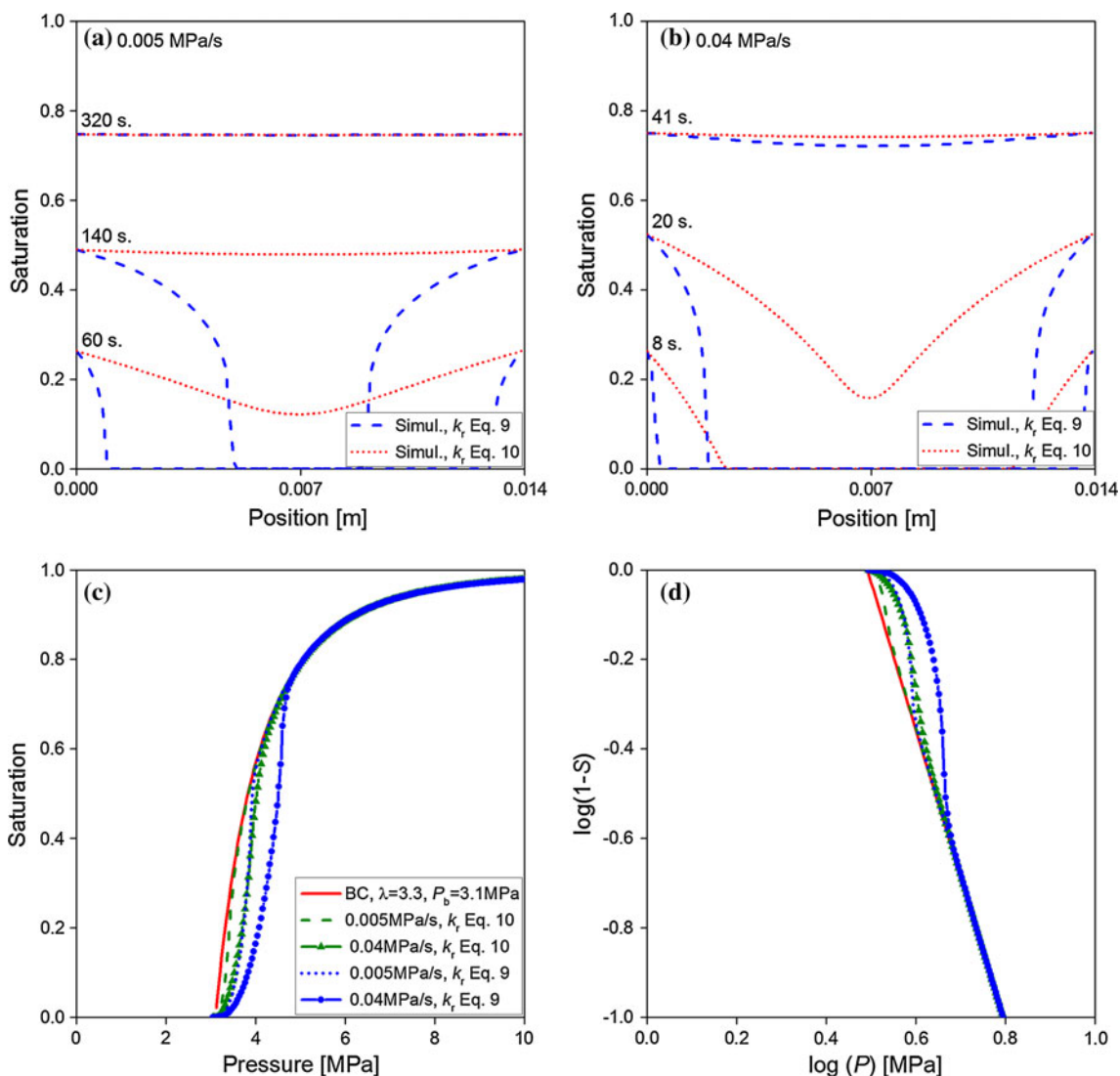
Fig. 8 Evolution of saturation across the preform depending on different conditions for relative permeability k_r given by Eqs. (9) and (10). For **a** 0.005 MPa/s after 60, 140, and 320 s (starting from P_b) and **b** 0.04 MPa/s after 8, 20, and 41 s. Corresponding drainage curves for **c** two pressurization rates, namely 0.005 and 0.04 MPa/s and **d** same data plotted in log $(1 - S)$ versus log (P). The numerical parameters are: $\lambda = 3.3$, $P_b = 3.1$ MPa, $k_s = 0.42 \times 10^{-14}$ m², $\mu = 3.6 \times 10^{-3}$ Pa s, and $V_r = 0.53$, calculated for radial infiltration of a cylinder of diameter 0.014 m. "BC" stands for the Brooks and Corey saturation curve used in the simulation (Eq. 7 with $\lambda = 3.3$, $P_b = 3.1$ MPa)

saturation for a different reason, namely the fact that capillarity and flow are, in the initial stages of infiltration, also governed by percolation [37, 42, 43].

Conclusion

- Improvements to the experimental procedures enable the exploration of an increased range of experimental conditions, including steady pressurization rates in the range 10^{-1}–10^{-4} MPa/s while maintaining stable high temperatures (1300 °C ± 5 °C) and tracking the displacement of the metal level with a precision of around

40–50 μm (for a total plunger displacement of 6 mm). With this apparatus, the entire drainage curve characterizing capillarity in high-temperature infiltration of porous preforms by molten metal can be obtained in a single experiment, using either continuous or stepwise pressurization. The technique gives stable results if pressurization rates at or below 0.04 MPa/s are used, suggesting in turn that such pressurization rates are in, or near, the range where infiltration is quasi-static. The present apparatus is essentially a high-temperature metal analogue of a mercury porosimeter; however, its function is somewhat different, in that a porosimeter is generally used to measure a pore size distribution
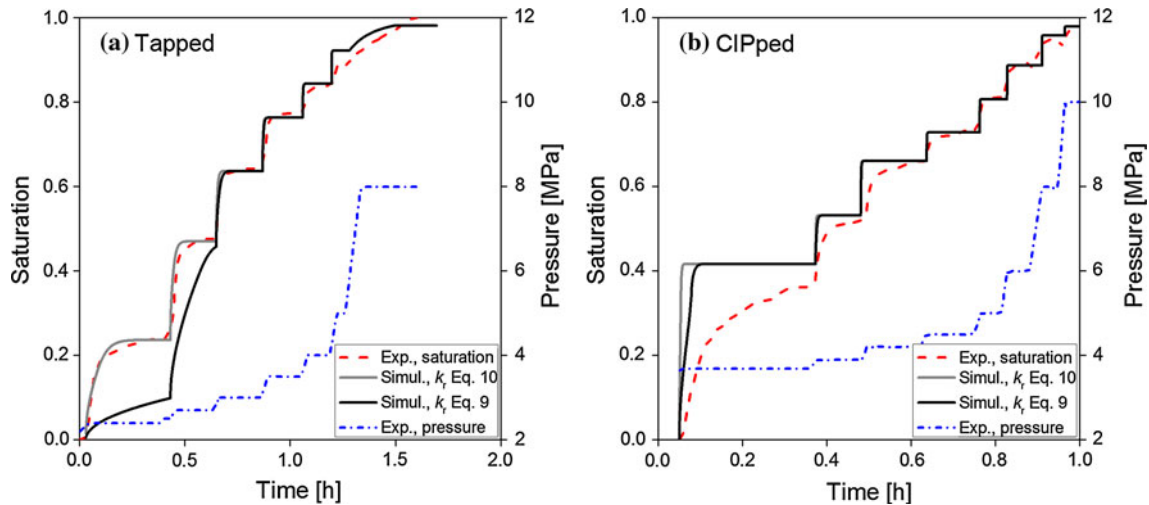
Fig. 9 Plot of pressure applied together with experimental and theoretically predicted curves of saturation as a function of time for **a** preform made by packing and vibrating ($\lambda = 3.1$, $P_b = 2.2$ MPa, $k_s = 0.7 \times 10^{-14}$ m^2, $\mu = 4.3 \times 10^{-3}$ Pa s, $V_r = 0.48$) and **b** preform made by CIP ($\lambda = 3.3$, $P_b = 3.1$ MPa, $k_s = 0.42 \times 10^{-14}$ m^2, $\mu = 3.9 \times 10^{-3}$ Pa s, $V_r = 0.53$). Infiltration temperature is **a** 1100 °C and **b** 1150 °C

(based on the assumption of a constant value for the contact angle of Hg), whereas the present apparatus is designed to measure wetting characteristics in various material systems (providing, thus, both capillary and geometric information).

- Semi-empirical equations derived in the context of soil science for flow of two immiscible fluids in a porous medium are applied to pressure infiltration of ceramic preforms with liquid metal. A finite difference code for the isothermal unidirectional infiltration of a rigid preform under any steadily increasing pressure function is implemented. Numerical and experimental results show good agreement for the alumina–copper system for two different pressurization rates if one takes the relative permeability equal to the saturation, as was proposed in ref [23]; comparatively, the expression given by Brooks and Corey underestimates infiltration rates significantly. A discrepancy between numerical and experimental results for stepwise infiltration of cold isostatically pressed preforms is, however, noted; this is the subject of future work.

References

1. Eustathopoulos N, Mortensen A (1993) In: Suresh S, Mortensen A, Needleman A (eds) Fundamentals of metal matrix composites. Butterworth-Heinemann, Stoneham, p 42
2. Mortensen A, Jin I (1992) Int Mater Rev 37:101.
3. Michaud VJ (1993) In: Suresh S, Mortensen A, Needleman A (eds) Fundamentals of metal matrix composites. Butterworth-Heinemann, Stoneham, p 3
4. Lloyd DJ, Morris AD, Jin I (1991) Melt process for the production of metal matrix composite materials with enhanced particle/matrix wetting. U.S 5,028,392
5. Mortensen A (2000) In: Clyne TW (ed) Comprehensive composite materials, vol 3. Pergamon, Oxford, p 521
6. Asthana R (1998) Solidification processing of reinforced metals. Trans-Tech Publications, Uetikon-Zurich
7. Evans A, SanMarchi C, Mortensen A (2003) Metal matrix composites in industry: an introduction and a survey. Kluwer Academic Publishers, Dordrecht
8. Michaud V, Mortensen A (2001) Compos A 32:981. doi:10.1016/S1359-835X(01)00015-X
9. Garcia-Cordovilla C, Louis E, Narciso J (1999) Acta Mater 47(18):4461. doi:10.1016/S1359-6454(99)00318-3
10. Chawla N, Chawla KK (2006) Metal matrix composites. Springer Verlag, New York
11. Adamson AW (1982) Physical chemistry of surfaces, 4th edn. Wiley, New York
12. Eustathopoulos N, Nicholas MG, Drevet B (1999) Wettability at high temperature. Pergamon-Elsevier Science, Amsterdam
13. deGennes PG, Brochard-Wyart F, Quéré D (2004) Capillarity and wetting phenomena: drops, bubbles, pearls, waves. Springer, New York (trans: Reisinger A)
14. Eustathopoulos N, Sobczak N, Passerone A, Nogi K (2005) J Mater Sci 40:2271. doi:10.1007/s10853-005-1945-4
15. Morrow NR (1970) Ind Eng Chem 62:32. doi:10.1021/ie50726a006
16. Bear J (1972) Dynamics of fluids in porous media. American Elsevier, New York
17. Michaud VJ, Compton L, Mortensen A (1994) Metall Trans A 25:2145. doi:10.1007/BF02652315
18. Bahraini M, Weber L, Narciso J, Mortensen A (2005) J Mater Sci 40:2487. doi:10.1007/s10853-005-1980-1
19. Molina JM, Narciso J, Louis E (2010) Scr Mater 62:961. doi:10.1016/j.scriptamat.2010.03.015
20. Michaud V, Mortensen A (2007) Scr Mater 56:859. doi:10.1016/j.scriptamat.2007.02.002

21. Mortensen A (1991) Mater Sci Eng A 135:1
22. Kaufmann H, Mortensen A (1992) Metall Trans A 23:2071. doi:10.1007/BF02647554
23. Dopler T, Modaressi A, Michaud VJ (2000) Metall Mater Trans B 31:225. doi:10.1007/s11663-000-0041-z
24. Bahraini M, Molina JM, Kida M, Weber L, Narciso J, Mortensen A (2005) Curr Opin Solid State Mater Sci 9:196. doi:10.1016/j.cossms.2006.02.007
25. Bahraini M, Molina JM, Weber L, Mortensen A (2008) Mater Sci Eng A 495:203. doi:10.1016/j.msea.2008.01.074
26. Kida M, Bahraini M, Molina JM, Weber L, Mortensen A (2008) Mater Sci Eng A 495:197. doi:10.1016/j.msea.2007.12.050
27. Dullien FAL (1979) Porous media, fluid transport and pore structure. Academic Press, New York
28. Bear J, Bachmat Y (1990) Introduction to modeling of transport phenomena in porous media. Kluwer Academic Publishers, Dordrecht
29. Rodriguez A, Sanchez S, Narciso J, Louis E, Rodriguez-Reinoso F (2005) J Mater Sci 40:2519. doi:10.1007/s10853-005-1985-9
30. Molina JM, Arpon R, Saravanan RA, GarciaCordovilla C, Louis E, Narciso J (2004) Scr Mater 51:623. doi:10.1016/j.scriptamat.2004.05.009
31. Molina JM, Prieto R, Duarte M, Narciso J, Louis E (2008) Scr Mater 59:243. doi:10.1016/j.scriptamat.2008.03.019
32. Molina JM, Rodriguez-Guerrero A, Bahraini M, Weber L, Narciso J, Rodriguez-Reinoso F, Louis E, Mortensen A (2007) Scr Mater 56:991. doi:10.1016/j.scriptamat.2007.01.042
33. Brooks RH, Corey AT (1964) Hydraulic properties of porous media, 3. Colorado State University Hydrology papers
34. Michaud VJ (2011) In: Boisse P (ed) Composite reinforcements for optimum performance. Woodhead Publishing, Oxford, p 431
35. Mortensen A, Masur LJ, Cornie JA, Flemings MC (1989) Theory Metall Trans A 20:2535. doi:10.1007/BF02666688
36. Mualem Y (1976) Water Resour Res 12(3):513. doi:10.1029/WR012i003p00513
37. Hunt A, Ewing R (2009) Percolation theory for flow in porous media. Springer, Heidelberg
38. Poirier DR, Geiger GH (1994) Transport phenomena in materials processing, 2nd edn. TMS, Warrendale
39. Gale WF, Totemeier TC (2004) Smithells metals reference book, 8th edn. Elsevier, Oxford
40. Bahraini M (2007) Characterization of capillary forces during liquid metal infiltration, EPFL doctoral thesis 3787. Ecole Polytechnique Fédérale de Lausanne, Lausanne
41. Higbie J (1991) Am J Phys 59:184
42. Sahimi M (1993) Rev Mod Phys 65:1393. doi:10.1103/RevModPhys.65.1393
43. Gouyet JF (1996) Physics and fractal structures. Masson, Paris and Springer, New York